AEROSOL OPTICAL DEPTH AS OBSERVED BY THE MARS SCIENCE LABORATORY REMS UV PHOTODIODES

M. D. Smith, *NASA Goddard Space Flight Center, Greenbelt, MD USA (Michael.D.Smith@nasa.gov)*, **M.-P. Zorzano,** *Luleå University of Technology, Kiruna, Sweden; CSIC-INTA, Madrid, Spain,* **M. Lemmon**, *Texas A&M University, College Station, TX,* **, J. Martín-Torres,** *Luleå University of Technology, Kiruna, Sweden; CSIC-UGR, Granada, Spain,* **T. Mendaza de Cal**, *Luleå University of Technology, Kiruna, Sweden.*

Introduction: Systematic observations taken by the REMS UV photodiodes on a daily basis throughout the landed Mars Science Laboratory mission provide a highly useful tool for characterizing aerosols above Gale Crater. Radiative transfer modeling is used to model the approximately two Mars Years of observations taken to date taking into account multiple scattering from aerosols and the extended field of view of the REMS UV photodiodes. The retrievals show in detail the annual cycle of aerosol optical depth, which is punctuated with numerous short timescale events of increased optical depth. Dust deposition onto the photodiodes is accounted for by comparison with aerosol optical depth derived from direct imaging of the Sun by Mastcam. The effect of dust on the photodiodes is noticeable, but does not dominate the signal. Cleaning of dust from the photodiodes was observed in the season around L_s=270°, but not during other seasons. Systematic deviations in the residuals from the retrieval fit are indicative of changes in aerosol effective particle size, with larger particles present during periods of increased optical depth. This seasonal dependence of aerosol particle size is expected as dust activity injects larger particles into the air, while larger aerosols settle out of the atmosphere more quickly leading to a smaller average particle size over time. A full description of these observations, the retrieval algorithm, and the results can be found in Smith et al. (2016).

Data Set: The Mars Science Laboratory (MSL) Curiosity rover has been operating on the surface of Mars in Gale Crater (4.59° S latitude, 137.44° E longitude) since August 2012 (Grotzinger et al., 2012). Here we use observations of UV radiative flux from the REMS instrument taken systematically each sol since the beginning of MSL landed operations, which cover more than two Martian years, from sol 9 (Mars Year 31, L_s=155°) to the present time.

One component of the REMS instrument suite (Gómez-Elvira et al., 2012) is a set of six photodiodes designed to measure UV flux (Zorzano et al., 2011). The photodiodes are mounted on the MSL rover deck facing directly upward to the sky. Each photodiode nominally views a cone centered straight upward from the rover deck with a 30° half-width from zenith. Five of the photodiodes cover narrow spectral bands (FWHM of 30-40 nm) with central wavelengths between 250 and 335 nm. The sixth photodiode is much wider covering the entire spectral range between 230 and 350 nm. Figure 1 shows the relative spectral response of the six REMS UV photodiodes.

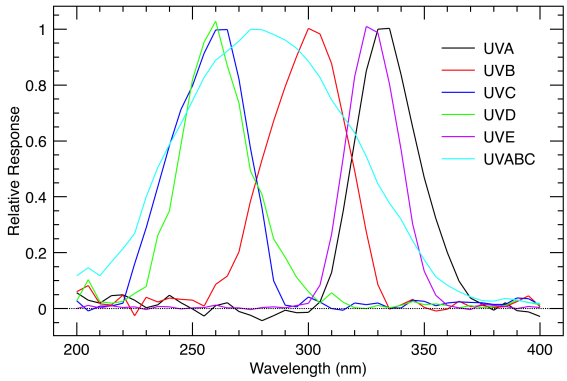

Figure 1. The spectral response of the six REMS UV photodiodes.

REMS UV observations are obtained systematically throughout each sol as part of a standard background observation set. The UV flux for each of the six photodiodes is recorded every second for the first five minutes of each Martian "hour," which is defined as one-twenty-fourth of a Martian sol. In addition, several additional hour-long blocks of continuous data are obtained each sol, with the timing of the blocks rotated though the sol to cover all local times over a time period of several sols. In general, in addition to the five-minute observations at the beginning of each hour, each sol has had at least three or four of the hour-long blocks during daylight hours when the UV data are useful.

Retrieval Algorithm: We use radiative transfer modeling of the observed UV signal in each photodiode to retrieve aerosol optical depth. For each photodiode, aerosol optical depth is retrieved by minimizing the least-squares difference between the observed and computed signals. Although it is possible to perform the retrieval on individual observations, we choose to use all the observations without shadows for a given sol with solar zenith angle less than 60° to retrieve a single optical depth for the sol. This provides for a robust retrieval with minimum uncertainty. Analysis of the residuals, or difference between observed and modeled signal, shows little systematic variation with local time caused by changes in aerosol optical depth within a sol.

The UV radiation observed by REMS comes from a combination of the direct solar beam (when the Sun is within the field of view) and the diffuse field of light scattered into the field of view by atmospheric aerosols (e.g., Zorzano and Córdoba-Jabonero, 2007; Zorzano et al., 2009). At these wavelengths, thermal radiation is negligible, and the observed signal does not depend on atmospheric temperature, surface temperature, or other surface properties.

To properly model the extended field of view and wavelength coverage of the REMS UV photodiodes, we compute the upward-looking radiance as viewed by the rover for a grid of zenith angle and azimuth angles in rover coordinates for each 5 nm wavelength between 200 and 400 nm. The spatial grid covers zenith angles from 0° to 70° in 1° increments, and azimuths from 0° to 359° in 1° increments. These are convolved with both the spectral response and the spatial response for each filter and integrated to find the total observed flux. The photodiode spectral response exhibits a weak dependence on instrument temperature with peak responses shifting to longer wavelengths at higher temperatures (Gómez-Elvira et al., 2012). This known temperature dependence is taken account of in the computation using the measured instrument temperature recorded by REMS.

Over time, dust settled onto the REMS UV photodiodes partially blocking their fields of view. We model this using a multiplicative factor that is a function of time (Fig. 2). This dust fallout calibration factor is determined using the set of derivations of aerosol optical depth obtained from direct imaging of the Sun by the Mastcam camera (e.g., Lemmon et al., 2015). These Mastcam measurements are nominally taken every three to seven sols and are of very high quality because of the direct nature of the observation.

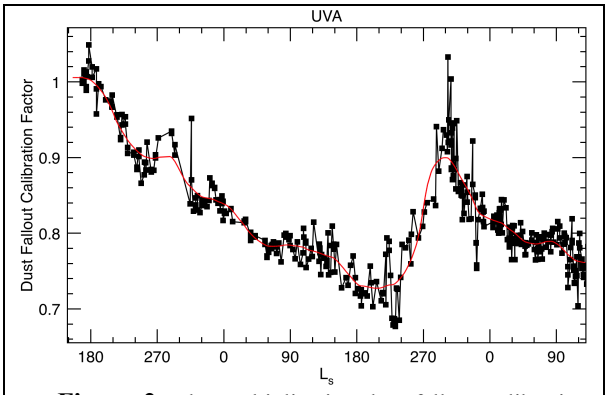

Figure 2. The multiplicative dust fallout calibration factor derived for each Mastcam image of the Sun (black points), and the smoothed representation (red line) that is used in the retrieval.

Results: Here we present results for the retrieval of aerosol optical depth from the REMS UV observations. The retrievals presented here cover approximately two Martian years of observations, from sols 9 to 1293 (MY 31, L_s=155° to MY 33, L_s=128°) including two full dust storm seasons. Aerosol optical depths are referenced to a wavelength of 880 nm, consistent with previously published values derived from direct imaging of the Sun (e.g., Lemmon et al., 2004; 2015).

Figure 3 shows the retrieved aerosol optical depths as a function of L_s. For clarity, only retrievals from the UVA, UVB, and UVE photodiodes are shown. Retrievals from the other three photodiodes are similar but have somewhat higher noise. The overall pattern as a function of season (L_s) is similar to what has been observed before by both orbiters (e.g., Smith et al., 2004; Smith 2009; McCleese et al., 2010; Kass et al., 2016) and rovers (e.g., Lemmon et al., 2004; 2015; Smith et al., 2006) for years without a global-scale dust storm.

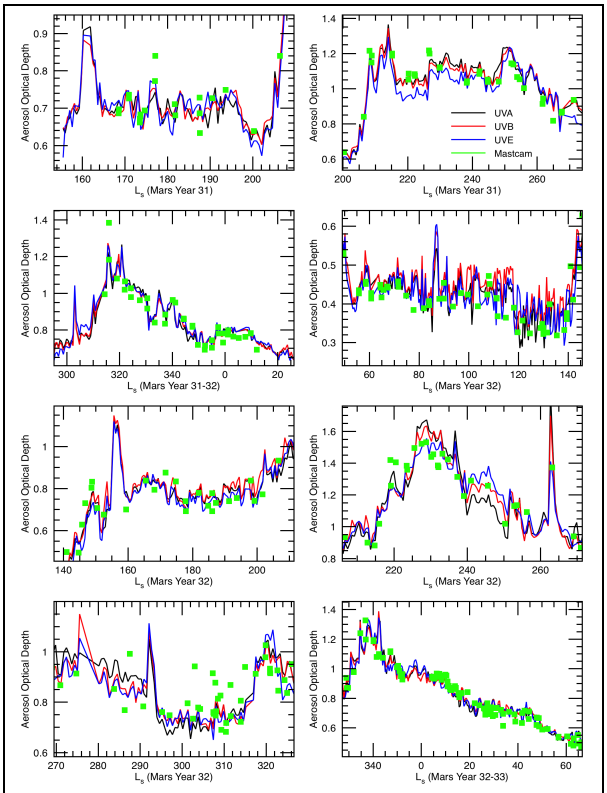

Figure 3. Comparison of the retrieved aerosol optical depth from the REMS UVA, UVB, and UVE photodiodes (black, red, and blue lines, respectively) with the aerosol optical depth derived from direct imaging of the Sun by Mastcam (green points). The overall seasonal cycle is punctuated by numerous significant increases in optical depth on short timescales that are often not characterized by Mastcam.

Short Timescale Variations in Daily Optical Depth: Figure 3 compares in detail the aerosol optical depth retrieved from the daily REMS UV photodiode observations against the periodic Mastcam images of the Sun. The high correlation between the three REMS UV retrievals shown argues for the validity of many of the small, short-timescale varia-

tions seen in the time series. Even when the retrieved optical depths from the three UV photodiodes diverge somewhat (e.g., MY 32, L_s=240°–250°) the sol-to-sol pattern in the retrievals remains the same.

It is clear that in numerous cases short-lived increases in aerosol optical depth lasting only one to three sols were completely missed by the Mastcam measurements. Prominent examples during MY 31 are at L_s=160°, 304°, 310°, and 335°. Examples during MY 32 are at L_s=87°, 156°, 237°, and 292°. At other times, Mastcam measurements showed increased optical depth, but the REMS UV retrievals "fill in" the gaps providing much greater detail about the evolution of the dust storms, for example at MY 31, L_s=210° and 320°, and throughout the MY 32, L_s=330°–350° period. In one case, an isolated Mastcam measurement that produced what might have been considered an anomalously high value at MY 32, L_s=263° is confirmed by the REMS UV retrievals to have been a real short-lived increase in optical depth. In a few cases, the REMS UV retrievals are able to fill in abnormally long gaps in the Mastcam record, such as MY 31, L_s=293°–314°, MY 32, L_s=12°–27°, and MY 32, L_s=352° to MY 33, L_s=4°. Each of those gaps in the Mastcam record of aerosol optical depth lasted more than three weeks. It is important to note that REMS was able to continue recording its hourly background observations even during the communication blackout period around solar conjunction, which was the cause of the first and last of the long gaps in the Mastcam record noted above.

The frequency of the short-lived increases in aerosol optical depth as a function of season is shown as the blue line in Fig. 4. An event is counted if the aerosol optical depth is more than 0.05 greater than a running average 5° of L_s wide. Although they can happen at any time of year, these short-timescale events are most common during the perihelion season (L_s=180°–360°) when overall dust optical depth is greatest. Indeed, none of the largest of these events with aerosol optical depth more than 0.10 greater than the running average have been observed during L_s=0°–135°. The fact that 23 of these short-lived increases in aerosol optical depth were observed per Mars Year, with many lasting just 2–3 sols, underscores the importance of the daily record of aerosol optical depth enabled by the REMS UV observations.

Figure 4 also compares the rate and seasonal dependence of short-lived increases in aerosol optical depth with those observed in the daily record from the *Spirit* and *Opportunity* rovers obtained using direct Pancam imaging of the Sun (Lemmon et al., 2004; 2015). There are significant differences between the three rovers. The seasonal dependence at *Opportunity* (Meridiani Planum) has a similar annual rate than at *Curiosity*, but there are more events earlier in the year (L_s=90°–180°). The seasonal dependence at *Spirit* (Gusev Crater) is markedly different with a lower overall rate except for a large spike in activity during the season L_s=135°–180°.

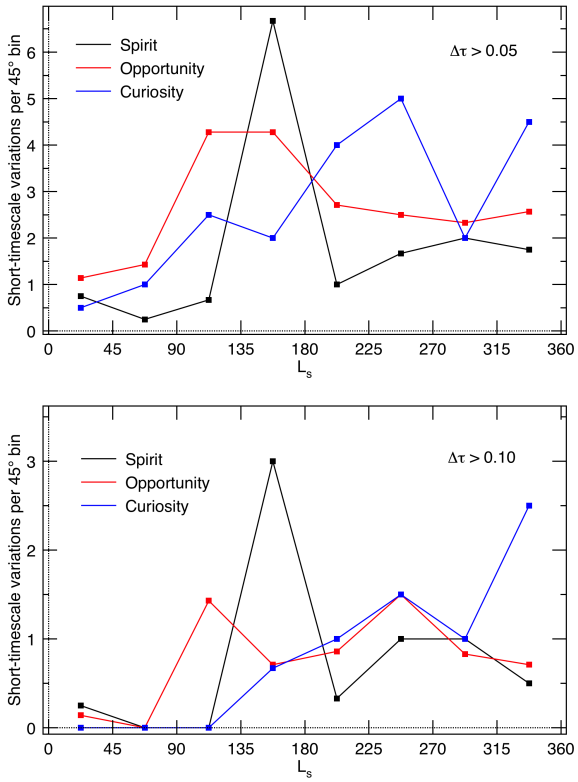

Figure 4. The frequency of short-lived events each Mars Year in a given bin of 45° of L_s. The upper panel shows the number of events with aerosol optical depth greater than 0.05 above the background level. The lower panel shows the number of events with aerosol optical depth greater than 0.10 above the background level.

Seasonal Dependence of Aerosol Size: Figure 5 shows the fractional residual for each individual REMS observation for the UVA, UVB, and UVE photodiodes for all sols. The fits are generally excellent, with fractional residuals (defined here as the observed signal minus the computed signal divided by the computed signal) less than a couple percent (i.e., green color in Fig. 5). However, at times there are systematic deviations in the fits on the order of 10–20%. These residuals are persistent over many sols and occur at consistent local times from sol to sol. There is also a high degree of correlation between the patterns in the residuals for the three photodiodes shown, which argues that the residuals are caused by a real physical effect not modeled by our initial assumptions.

The likely cause for the residuals is that the aerosol physical properties are not constant for all seasons and local times as we have assumed. The change in the aerosol physical properties could be a change in the composition (i.e., the relative mixing of dust vs. water ice aerosol), or in the aerosol particle size. There are strong reasons to conclude that this is the case rather than a change in the aerosol optical depth. There are several systematic trends in

Fig. 5 that are common to the three REMS UV photodiodes. There is a clear tendency for the residuals to be symmetric about noon local time, with the residuals most apparent in the earliest (before 9:30) and latest (after 14:30) observations. It is possible that aerosol optical depth could change symmetrically about noon, but the more simple explanation is that this is a dependence on solar zenith angle, not local time, which would point to the cause being from a change in aerosol physical properties. Furthermore, the largest residuals occur during L_s=210°–260° and 320°–350° in both Mars Years, which is exactly the period during which there was increased dust activity and the highest aerosol optical depth (Fig. 3). Therefore, the residuals are most likely related to changes in aerosol physical properties caused by the increased dust activity.

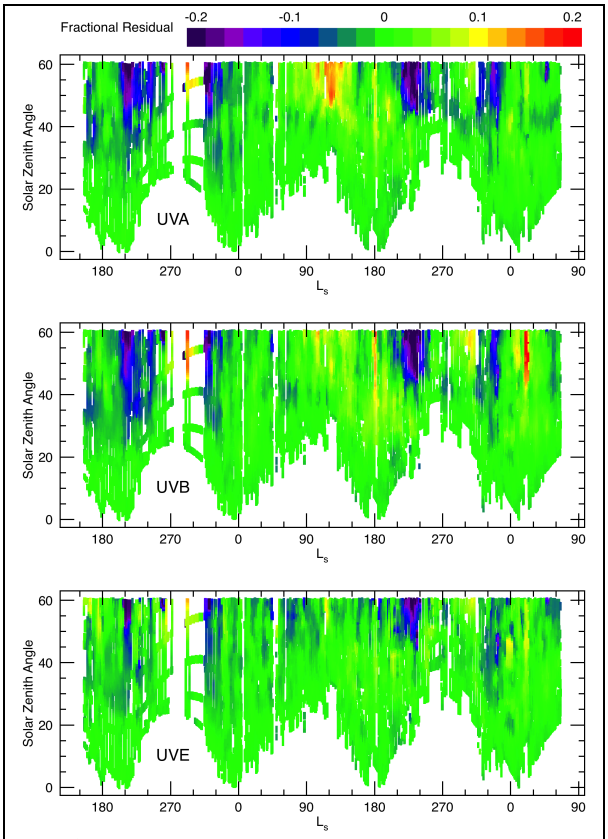

Figure 5. The residuals from the retrieval of aerosol optical depth for the UVA, UVB, and UVE photodiodes as a function of L_s and solar zenith angle. The clear seasonal variation in residuals at high solar zenith angle are associated with the timing of increased aerosol optical depth and are indicative of changes in the aerosol effective particle size.

The residuals remain very small within the nominal field of view of the photodiodes (solar zenith angle less than 30°), and rapidly grow to about 20% at the highest solar zenith angles. The most straightforward change to aerosol physical properties that causes this type of variation is a change in aerosol particle size. A residual of -20% could be caused by dust particles that had effective radius 2.5 µm instead of the assumed 1.5 µm. This amount of variation in aerosol particle size is consistent with previous studies from the Mars Exploration Rovers (Wolff et al., 2006; Lemmon et al., 2015) and from orbiters (Wolff and Clancy, 2003; Guzewich et al., 2014).

It is not possible to uniquely determine the aerosol particle size from these residuals since any mismatch in the baseline or time-averaged particle size from the 1.5 µm that was assumed will be compensated for in the spatial response functions that we derive. However, it can be concluded from these data that the aerosol particle size increased (leading to negative residuals) during the times of dust activity when retrieved aerosol optical depth was highest, and that the increase in effective particle radius was about 60%. There is also a suggestion in Fig. 5 that there are generally positive residuals at high solar zenith angles between L_s=60° and 150°, which would imply smaller effective particle radius during that season. This seasonal dependence of aerosol particle size is expected as dust activity injects larger particles into the air, while larger aerosols settle out of the atmosphere more quickly leading to a smaller average particle size over time (Kahre et al., 2008).

References:

Gómez-Elvira, J., *et al.* (2012). *Space Sci. Rev.*, **170**, 583–640.

Grotzinger, J.P. *et al.* (2012). *Space Sci. Rev.*, **170**, 5–56.

Guzewich, S.D., *et al.* (2014). *J. Geophys. Res.,* **119**, 2694–2708, doi:10.1002/2014JE004704.

Kahre, M.A., *et al.* (2008). *Icarus*, **195**, 576–597.

Kass, D.M., *et al.* (2016). *Geophys. Res. Lett.*, **43**, doi:10.1002/2016GL068978.

Lemmon, M. T., *et al.* (2004). *Science*, **306**, 1753–1756.

Lemmon, M.T., *et al.* (2015). *Icarus*, **251**, 96–111.

McCleese, D.J., *et al.* (2010). *J. Geophys. Res.*, **115**, E12016, doi:10.1029/2010JE003677.

Smith, M.D. (2004), *Icarus*, **167**, 148–165.

Smith, M.D. (2009), *Icarus,* **202**, 444–452.

Smith, M.D., *et al.* (2006). *J. Geophys. Res.*, **111**, E12S13, doi:10.1029/2006JE02770.

Smith, M.D., *et al.* (2016). *Icarus*, **280**, 234–248.

Wolff, M. J., and R. T. Clancy (2003). *J. Geophys. Res.*, **108**, E9, 5097, doi:10.1029/2003JE002057.

Wolff, M. J., *et al.* (2006). *J. Geophys. Res.*, **111**, E12S17, doi:10.1029/2006JE002786.

Zorzano, M.-P. *et al.* (2007). *Icarus*, **190**, 495–503.

Zorzano, M.-P. *et al.* (2009). *Inverse Prob.*, **25**, 115023, doi:10.1088/0266-5611/25/11/115023.

Zorzano, M.-P., *et al.* (2011). ISBN:978-953-307-277-7.